



# Electronic Conductive Inorganic Cathodes Promising High-Energy Organic Batteries

Minglei Mao, Shu Wang, Zejing Lin, Tao Liu, Yong-Sheng Hu, Hong Li, Xuejie Huang, Liquan Chen, and Liumin Suo\*

The electrochemical utilization of organic electrode materials (OEMs) is highly dependent on an excess amount of inactive carbon at the expense of low packing density and energy density. In this work, the challenges by substituting inactive carbon with electronic conductive inorganic cathode (ECIC) materials, which are endowed with high electronic conductivity to transport electrons for redox reactions of the whole electrodes, high ion-storage capacity to act as secondary active materials, and strong affinity with OEMs to inhibit their dissolution, are addressed. Combining representative ECICs ( $TiS_2$  and  $Mo_6S_8$ ) with organic electrode materials (perylene-3,4,9,10-tetracarboxylic dianhydride (PTCDA) and hexaazatrinaphthalene (HATN)) simultaneously achieves high capacity, low porosity, lean electrolyte, and thus high energy density. High gravimetric and volumetric energy densities of 153 Wh kg<sup>-1</sup> and 200 Wh L<sup>-1</sup> are delivered with superior cycling stability in a 30 mA h-level Li/PTCDA- $TiS_2$  pouch cell. The proof-of-concept of organic-ECIC electrodes is also successfully demonstrated in monovalent Na, divalent Mg, and trivalent Al batteries, indicating their feasibility and generalizability. With the discovery of more ECIC materials and OEMs, it is anticipated that the proposed organic-ECIC system can result in further improvements at cell level to compete with transition metal-based Li-ion batteries.

Over the past few decades, Li-ion battery (LIB) technology has revolutionized portable devices and electric vehicles, owing to substantial improvements and notably the development of new intercalation cathode materials.<sup>[1]</sup> However, the boom in the

LIB industry poses enormous pressure on expensive metals, especially Co and Ni. Redox-active organic species can relieve this pressure and offer valid options in terms of environmental footprint and possible disruptive chemistries,<sup>[2]</sup> because they are mainly composed of C, H, O, N, and S, which are naturally abundant elements as well as the main constituents of biomass.<sup>[3]</sup> Significant progress has been achieved in exploiting new organic electrode materials and modifying existing organic materials.<sup>[4]</sup> Still, the advance of organic electrode materials (OEMs) is severely constrained by intrinsically poor electronic conductivity and low energy density.

A high fraction of conductive carbon addition (20–50 wt%) is necessary for sufficient OEM use in conventional organic electrodes.<sup>[3a,4a,d,5]</sup> Nevertheless, the use of an excess amount of high-specific-area carbon gives rise to high electrode porosity, which demands a considerable amount of electrolyte to support a satisfac-

tory ionic conductivity. Herein, we investigate the relationships between carbon content, porosity, and energy density by using perylene-3,4,9,10-tetracarboxylic dianhydride (PTCDA),<sup>[6]</sup> one of the most representative OEMs, as an example (Figure 1). When the ratio of active material (PTCDA) in the electrodes increases from 60% to 95% (implying a decrease from 30% to 3% of carbon content), the porosity of the electrodes decreases from 79.4% to 45.9%, concomitant with an E/AM (active material) drop from 3.4 to 0.51  $\mu$ L mg<sup>-1</sup> (Figure 1a). Accordingly, the predicted gravimetric energy density of the electrodes undergoes a remarkable 255% increase (from 56.1 to 199.2 Wh kg<sup>-1</sup>) and the volumetric energy density 285% (from 79.9 to 307.8 Wh L<sup>-1</sup>) (Figure 1b). Note that a temerarious increase in AM ratio will inevitably impair the utilization of OEMs, compromising the elevation in theoretical energy density. The balance between sufficient utilization of OEMs and a reduction in the inactive carbon addition is a dilemma.

To circumvent this dilemma, a multifunctional material endowed with high electronic conductivity should be applied to substitute carbon and act as part of the active materials, to guarantee high utilization of OEMs and high ion-storage capability. Accordingly, we narrowed the scope to intercalation inorganic cathode materials with high electronic conductivity.

Dr. M. Mao, S. Wang, Z. Lin, Dr. T. Liu, Prof. Y. Hu, Prof. H. Li, Prof. X. Huang, Prof. L. Chen, Prof. L. Suo  
Beijing Advanced Innovation Center for Materials Genome Engineering  
Key Laboratory for Renewable Energy  
Beijing Key Laboratory for New Energy Materials and Devices  
Institute of Physics  
Chinese Academy of Sciences  
Beijing 100190, China  
E-mail: suolumin@iphy.ac.cn

S. Wang, Prof. L. Suo  
Center of Materials Science and Optoelectronics Engineering  
University of Chinese Academy of Sciences  
Beijing 100049, China

Prof. L. Suo  
Yangtze River Delta Physics Research Center Co. Ltd.  
Liyang, Jiangsu 213300, China

The ORCID identification number(s) for the author(s) of this article can be found under <https://doi.org/10.1002/adma.202005781>.

DOI: 10.1002/adma.202005781

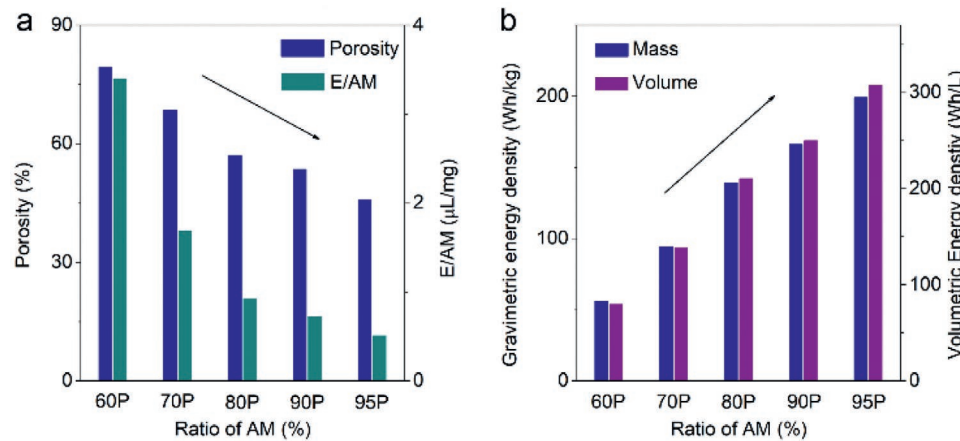


**Figure 1.** Design strategy for high-energy organic electrodes. a,b) The relationship of porosity and E/AM (electrolyte/active materials) (a), as well as predicted gravimetric and volumetric energy density versus AM ratio (b). These calculations are based on PTCDA electrodes in LIBs. xP ( $x = 60, 70, 80, 90$ , and  $95$ ) means the ratio of PTCDA in electrodes. We calculate the electrolyte amount by assuming that all the porosity in the cathode is filled by electrolyte. For calculation details refer to Table S1 of the Supporting Information.

Representative cathode materials were screened (Figure 2a), in which Li-containing oxide cathode materials ( $\text{LiMn}_2\text{O}_4$ ,<sup>[7]</sup>  $\text{LiVPO}_4\text{F}$ ,<sup>[8]</sup>  $\text{LiCoO}_2$ ,<sup>[9]</sup> and  $\text{LiFePO}_4$ ,<sup>[10]</sup>) were excluded due to a working voltage outside the range of most OEMs (1.5–3 V vs Li/Li<sup>+</sup>, the cyan region in Figure 2a,b<sup>[4a,11]</sup>). Other oxides ( $\text{V}_2\text{O}_5$ ,<sup>[12]</sup>  $\text{MoO}_3$ ,<sup>[13]</sup> and  $\text{TiO}_2$ ,<sup>[14]</sup>) and some sulfides ( $\text{MoS}_2$ ,<sup>[15]</sup>  $\text{NbS}_2$ ,<sup>[16]</sup> and  $\text{WS}_2$ ,<sup>[17]</sup>) were removed because of their low electronic conductivity. The other sulfides ( $\text{Mo}_6\text{S}_8$ ,<sup>[18]</sup>  $\text{TiS}_2$ ,<sup>[19]</sup> and  $\text{NbS}_3$ ,<sup>[20]</sup>) and selenides ( $\text{TiSe}_2$ ,<sup>[21]</sup>  $\text{VSe}_2$ ,<sup>[22]</sup> and  $\text{NbSe}_2$ ,<sup>[23]</sup>) are reported to have both high electronic conductivity and ion-storage capacities,<sup>[24]</sup> with appropriate working potentials (1.5–3 V vs Li/Li<sup>+</sup>).

In this study, Chevrel phase  $\text{Mo}_6\text{S}_8$  and layered  $\text{TiS}_2$  (Figure S1, Supporting Information) were selected as representative electronic conductive inorganic cathode (ECIC) materials paired with organic PTCDA and hexaazatrinaphthalene (HATN) (Figure 2b) to form organic + ECIC composites (O-ECIC). The powder conductivity of ECIC was first investigated by the four-pin probe method. The conductivities of  $\text{Mo}_6\text{S}_8$  (83.1 S cm<sup>-1</sup>) and  $\text{TiS}_2$  (74.4 S cm<sup>-1</sup>) are even higher than those of widely utilized conductive Ketjenblack (31.6 S cm<sup>-1</sup>) and super P (46.5 S cm<sup>-1</sup>) (Figure 2c). Further, the conductivity of PTCDA- $\text{Mo}_6\text{S}_8$  (P-MS) (0.62 S cm<sup>-1</sup>) and PTCDA- $\text{TiS}_2$  (P-TS) (0.73 S cm<sup>-1</sup>) were measured to be higher than those of 80P (0.12 S cm<sup>-1</sup>) and 90P (nondetectable), which are sufficient in commercial application of batteries.<sup>[25]</sup>

In traditional organic/carbon electrodes, insulative OEMs can only receive electrons from conductive carbon (Figure 2d). Excessive carbon content is necessary to guarantee an efficient conductive network, which not only diminishes the ratio of active OEMs in the electrodes but also increases the porosity of the electrodes and electrolyte addition to maintain acceptable rate capability (Figure S3a,c, Supporting Information). It significantly compromises the specific energy and energy density of traditional organic/carbon electrodes. While in our proposed O-ECIC electrodes, OEMs are able to acquire electrons from both carbon and ECIC (step I), concomitant with Li<sup>+</sup> intercalation into the secondary ECIC active material (step II). Our

O-ECIC design achieves a compact electrode with a high ratio of active materials (OEM + ECIC) (Figure S3b,d, Supporting Information), considerably reducing the inactive carbon content, electrode porosity, and electrolyte addition. Thus, high specific energy and energy density are expected.

When applied in LIBs, variation in the chemical composition of O-ECIC electrodes was first studied during the discharge/charge process. The multiple redox processes of P-MS can be clearly observed by cyclic voltammetry (CV) (Figure 3a). The cathodic peaks at 2.65, 2.48, and 2.35 V represent the stepwise reduction of PTCDA (Figure S5a, Supporting Information),<sup>[11c]</sup> while the peaks at 2.43, 2.03, and 1.81 V are due to the formation of  $\text{LiMo}_6\text{S}_8$ ,  $\text{Li}_3\text{Mo}_6\text{S}_8$ , and  $\text{Li}_4\text{Mo}_6\text{S}_8$  (Figure S5b, Supporting Information). In the reverse scan during charging,  $\text{Li}_x\text{Mo}_6\text{S}_8$  ( $x = 0, 1, 3$ , and  $4$ ) sequentially deintercalates all the Li<sup>+</sup> to reform  $\text{Mo}_6\text{S}_8$ , followed by Li<sup>+</sup> extraction from  $\text{Li}_y(\text{PTCDA})$  ( $0 \leq y \leq 2$ ). Likewise, P-TS electrodes undergo a similar process in CV measurement (Figure S5c,d, Supporting Information). To gain insight into the phase evolution of P-MS during the discharge/charge processes, operando XRD patterns were collected in the range of 1.5–3 V (Figure 3b,c; Figure S7, Supporting Information). Only peaks corresponding to  $\text{Li}_x\text{Mo}_6\text{S}_8$  can be observed, with no peaks for PTCDA, which can be ascribed to the lower crystallinity of organic PTCDA compared to that of inorganic  $\text{Li}_x\text{Mo}_6\text{S}_8$ . At the beginning of discharge, the reflections indexed to rhombohedral  $\text{Mo}_6\text{S}_8$  (JCPDS: 89–5114) remain steady. As the discharge proceeds to 2.43 V, four characteristic peaks located at 13.7°, 33.9°, 46.7°, and 52.7° shift toward lower angles corresponding to rhombohedral  $\text{LiMo}_6\text{S}_8$  (JCPDS: 81–0858) (Figure 3c; Figure S7, Supporting Information). Further discharged to 2.03 and 1.81 V, there is an apparent phase transformation with peaks assigned to  $\text{Li}_3\text{Mo}_6\text{S}_8$  (JCPDS: 81–0859) and  $\text{Li}_4\text{Mo}_6\text{S}_8$  (JCPDS: 81–0860), respectively. During the recharging process, all reflections evolve before 2.5 V and remain unchanged until the end of the charge, in accordance with the CV results.

The constant variation of  $\text{Mo}_6\text{S}_8$  compositions necessitates the evaluation of its conductivity in various states, in which

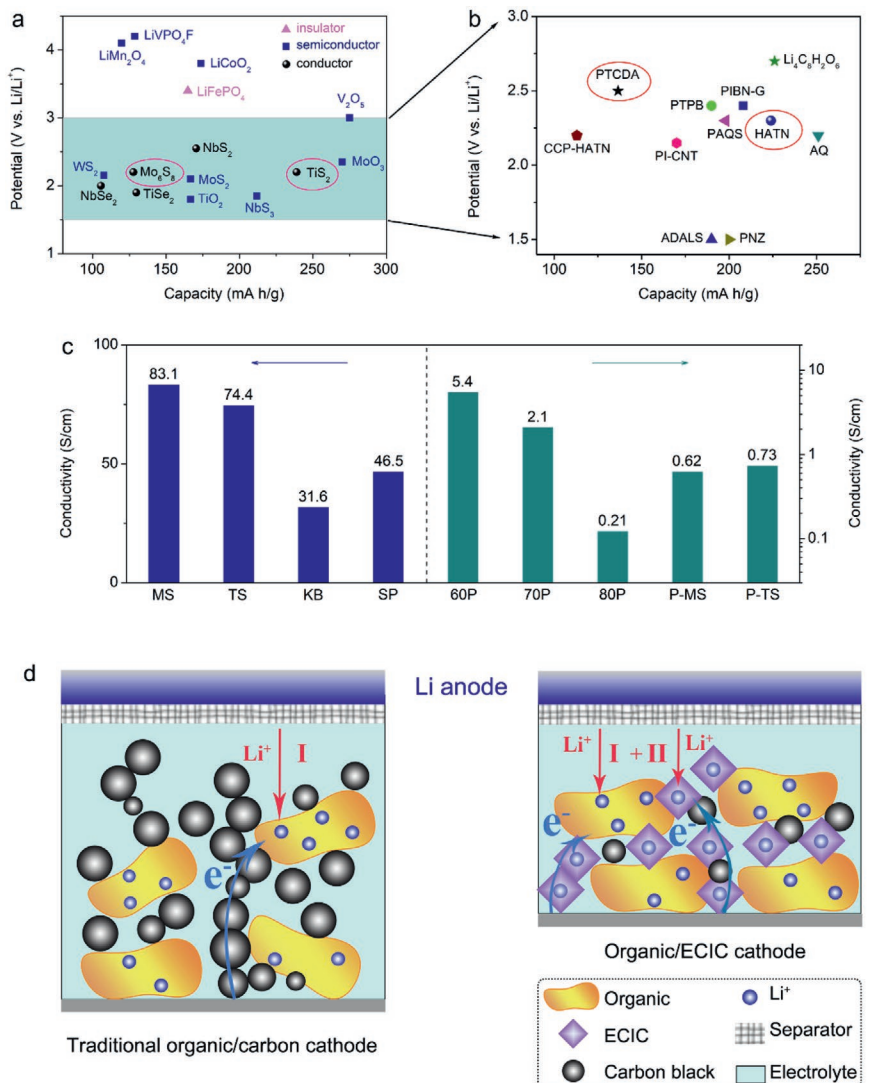


**Figure 2.** Configuration of O-ECIC systems. a) Screening electronic conductive inorganic cathode (ECIC) materials. The cyan region between 1.5 and 3 V versus Li/Li<sup>+</sup> represents the working potential of most organic electrode materials. The magenta triangle, navy squares, and black balls represent insulators, semiconductors, and conductors, respectively. Mo<sub>6</sub>S<sub>8</sub> and TiS<sub>2</sub> in the pink circles are selected as representative ECICs in this work. b) Comparison of reported OEMs in terms of capacity and potential. PTCDA and HATN in the red circles are chosen as representative organic materials in this work. c) Investigation of electronic conductivity of Mo<sub>6</sub>S<sub>8</sub>, TiS<sub>2</sub>, Ketjenblack (KB), and Super P (SP) powders and 60–80P, P-MS, and P-TS powders using four-pin probe method. P-MS/TS refers to 60% PTCDA + 30% Mo<sub>6</sub>S<sub>8</sub>/TiS<sub>2</sub> in electrodes. For details, refer to Tables S2 and S3 of the Supporting Information. d) Illustration of organic-based LIBs, including traditional organic/carbon electrodes and O-ECIC electrodes. The blue and red arrows refer to the pathways of electrons and Li<sup>+</sup> insertion into organic materials and ECIC, respectively. The porosity and packing density of the O-ECIC electrode are far superior to those of traditional organic/carbon cathodes.

density of states (DOS) of  $\text{Li}_x\text{Mo}_6\text{S}_8$  ( $x = 0, 1, 3$ , and  $4$ ) was determined using first-principles calculations (Figure 3d; Figure S8, Supporting Information). Through the discharge process from the initial form ( $\text{Mo}_6\text{S}_8$ ) to its final form ( $\text{Li}_4\text{Mo}_6\text{S}_8$ ),  $\text{Li}_x\text{Mo}_6\text{S}_8$  maintain high electronic conductivity, demonstrating that an efficient conductive network can be guaranteed for the entire redox process of the O-ECIC composite electrodes. In situ electrochemical impedance spectroscopy was also conducted to confirm this. During the lithiation/delithiation of either PTCDA or  $\text{Mo}_6\text{S}_8$ , the resistance of electrode reaction did not change significantly (Figure S10, Supporting Information). In addition to providing a conductive network and Li-storage capacity, ECIC

also has a strong affinity with OEMs to inhibit their dissolution. This is important for OEMs because dissolution issues, especially for lithiated OEMs, are a severe challenge for their application. The binding energy of  $\text{Li}_x\text{Mo}_6\text{S}_8$  with  $\text{Li}_2\text{PTCDA}$  was calculated (Figure 3e), in which all species  $\text{Li}_x\text{Mo}_6\text{S}_8$  from  $\text{Mo}_6\text{S}_8$  (2.75 eV) to  $\text{Li}_4\text{Mo}_6\text{S}_8$  (3.85 eV) have a strong affinity for  $\text{Li}_2\text{PTCDA}$ . By contrast, commonly used conductive carbon has much less interaction with  $\text{Li}_2\text{PTCDA}$  (1.51 eV) (Figure 3f). The strong affinity of  $\text{Li}_x\text{Mo}_6\text{S}_8$  for OEMs will restrain their dissolution in the electrolyte, contributing to cycling stability.

The electrochemical performance of the PTCDA/carbon, P-TS, and P-MS electrodes was evaluated using coin cells

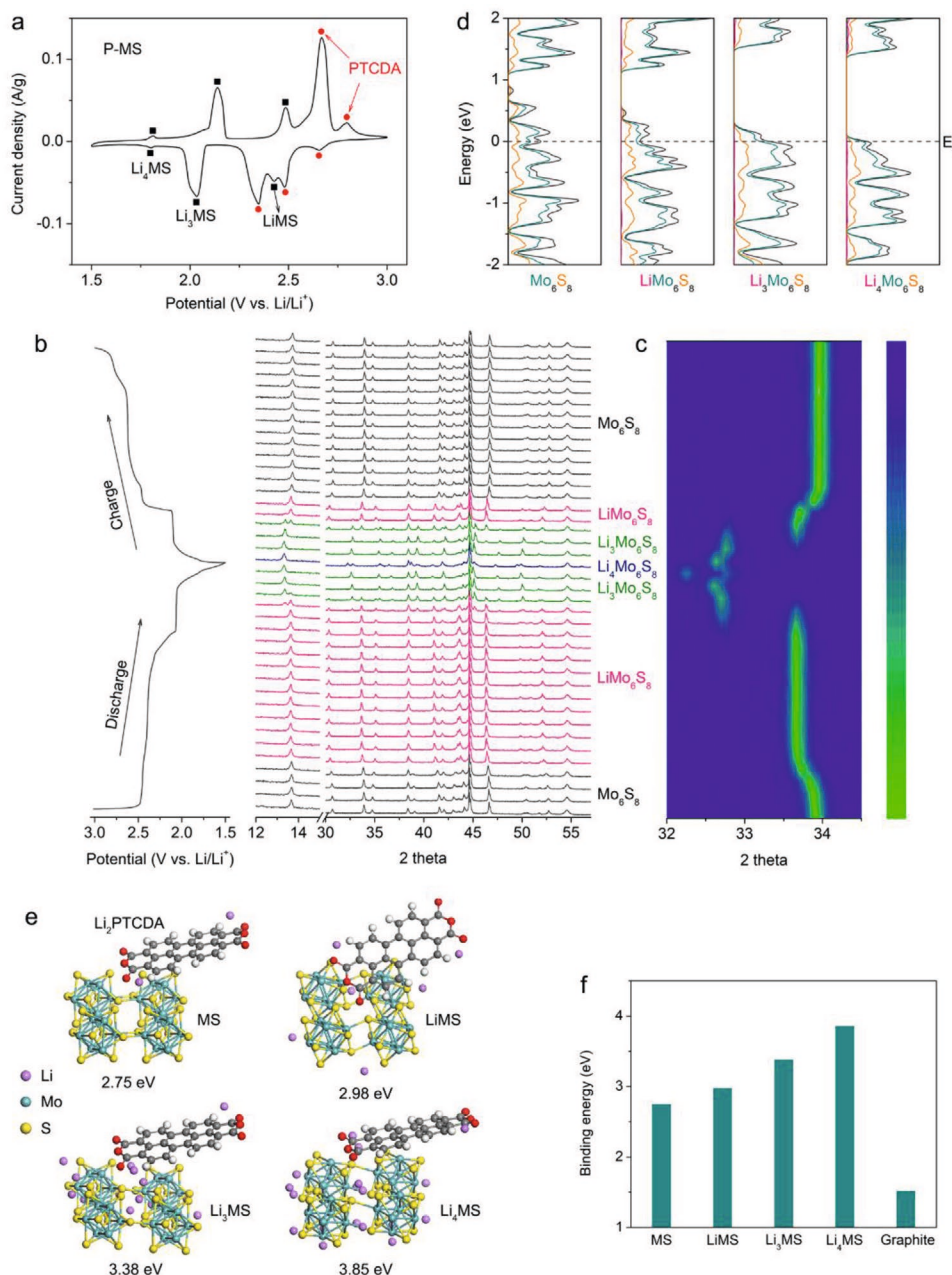


**Figure 3.** Investigation of redox mechanism of P-MS. a) Cyclic voltammetry of P-MS at a scan rate of  $0.05 \text{ mV s}^{-1}$  between 1.5 and 3 V. b) Operando XRD patterns collected during the first discharge/charge of Li/P-MS cells at  $100 \text{ mA g}^{-1}$  between 1.5 and 3 V. c) Corresponding contour map of operando XRD patterns. d) Evolution of density of states (DOS) of  $\text{Li}_x\text{Mo}_6\text{S}_8$  ( $x = 0, 1, 3, \text{ and } 4$ ). Li, Mo, and S projections are colored in pink, cyan, and orange, respectively. e) Relaxed structures of  $\text{Li}_2\text{PTCDA}$  adsorption on the  $\text{Li}_x\text{Mo}_6\text{S}_8$  surfaces using density functional theory calculations. f) Comparison of binding energies of  $\text{Li}_x\text{Mo}_6\text{S}_8$  and graphite with  $\text{Li}_2\text{PTCDA}$ .

with  $3 \text{ mol L}^{-1}$  LiTFSI in DME electrolyte between 1.5 and 3 V (Figure 4). At  $100 \text{ mA g}^{-1}$ , P-TS and P-MS delivered capacities of  $134$  and  $110 \text{ mA h g}^{-1}$  (based on the total mass of the electrodes), respectively, which are much higher than those of all the PTCDA/carbon electrodes (Figure 4a). Although 60P exhibits a higher capacity of  $129.2 \text{ mA h g}^{-1}$  based on the active material (PTCDA), the excessive carbon addition compromises the capacity delivery based on the whole electrode ( $77.5 \text{ mA h g}^{-1}$ ) (Figure 4b). P-TS and P-MS showed superior cycling stability

with capacity retentions of  $92.6\%$  and  $94.4\%$  after 200 cycles, respectively, and the average coulombic efficiency approaching  $99.8\%$  (Figure 4c). The rate capability of P-MS was further evaluated at various current densities from  $20$  to  $2000 \text{ mA g}^{-1}$  (Figure 4d). When the current density increased from  $20$  to  $500 \text{ mA g}^{-1}$ , the capacity of P-MS decreased slightly from  $130$  to  $110 \text{ mA h g}^{-1}$  with a marginal increase in voltage hysteresis, indicative of fast redox kinetics (Figure S13, Supporting Information). Even at ultrahigh current densities of  $1000$  ( $8 \text{ C}$ )

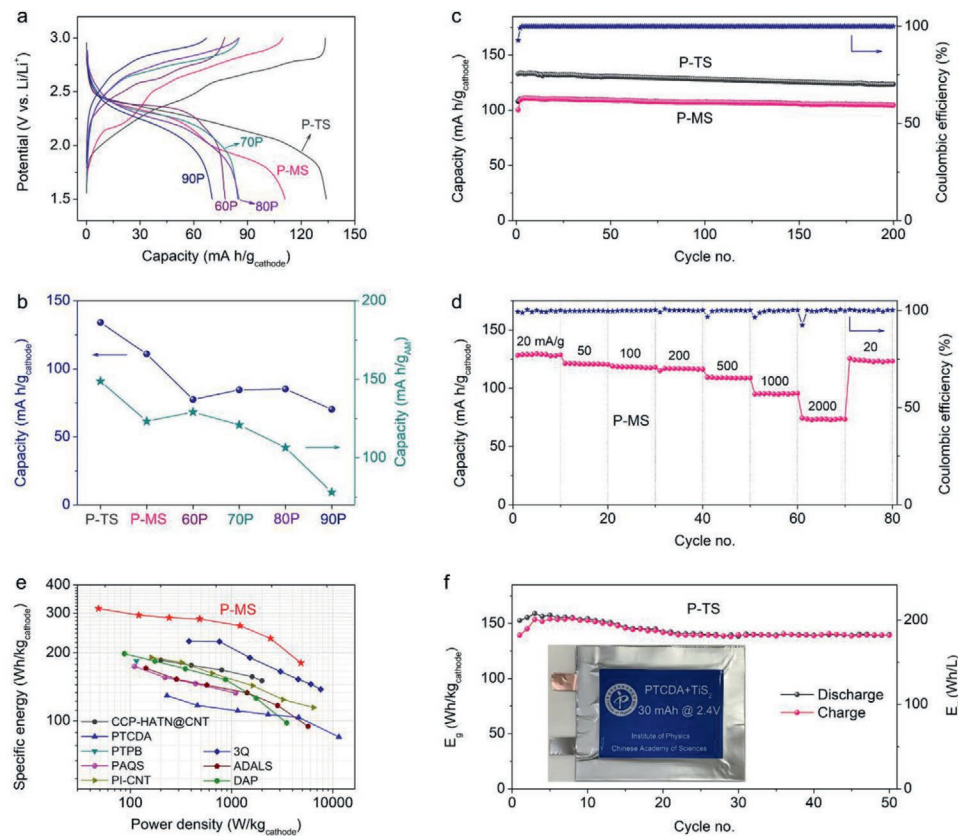


**Figure 4.** Electrochemical performance of PTCDA and O-ECIC electrodes with  $3 \text{ mol L}^{-1}$  LiTFSI in DME electrolyte between 1.5 and 3 V in LIBs. a) Typical discharge/charge curves at  $100 \text{ mA g}^{-1}$ . b) Capacity comparison based on the mass of active materials and the whole cathodes. c) Cycling performance of P-TS and P-MS at  $100 \text{ mA g}^{-1}$  for 200 cycles. d) Rate performance of P-MS with current densities varying from 20 to  $2000 \text{ mA g}^{-1}$ . e) Ragone plot of Li/P-MS coin cells compared with previously reported OEMs for LIBs. f) Cycling performance of Li/P-TS pouch cells with a high capacity of  $30 \text{ mA h}$  and areal mass loading of  $\approx 8 \text{ mg cm}^{-2}$ . All the specific capacities in coin cells are calculated based on the total mass of cathodes, including active materials (organic materials and ECIC), conductive addition, and binder. The gravimetric and volumetric energy density of pouch cells are calculated with 50% excess Li metal anode, cathode, electrolyte, current collector, and separator all included.

and  $2000 \text{ mA g}^{-1}$  (16 C), P-MS still retained capacities of 95.4 and  $73.5 \text{ mA h g}^{-1}$ , respectively, which immediately recovered to  $124 \text{ mA h g}^{-1}$  at a current density of  $20 \text{ mA g}^{-1}$  (Figure 4d). Remarkable specific energies were achieved for P-MS electrodes throughout a wide range of rates, outperforming reported high-performance OEMs (Figure 4e).<sup>[4a,11a-d,f-i]</sup> The Ragone plot shows that a specific energy of  $180 \text{ Wh kg}^{-1}$  is delivered within 3.6 min, corresponding to a specific power of  $4840 \text{ W kg}^{-1}$ . To further exploit the practical potential of the O-ECIC system, a  $30 \text{ mA h}$ -level pouch cell was assembled with a 50% excess Li metal anode, which shows superior cycling performance with a joint high specific energy ( $140 \text{ Wh kg}^{-1}$ ) and energy density ( $183 \text{ Wh L}^{-1}$ ) at a cell level at  $0.2 \text{ mA cm}^{-2}$  after 50 cycles (Figure 4f; Figure S16, Supporting Information). To the best of our knowledge, our full-cell joint  $E_g$ – $E_v$  represents a very high level among reported Li-organic systems.<sup>[2a,26]</sup> It is worth noting that, after optimizing the production process of pouch cells, it is expected that further enhancement of  $E_g$  and  $E_v$  of O-ECIC systems is possible.

To validate the universality of our proposed O-ECIC systems, we evaluated O-ECIC electrodes beyond Li systems (Figures S17–S19, Supporting Information). In Na-ion batteries, P-TS and P-MS delivered capacities of  $130.5$  and  $104.4 \text{ mA h g}^{-1}$ ,

respectively, much higher than those of PTCDA/carbon electrodes ( $<75 \text{ mA h g}^{-1}$ ) (Figure S17a, Supporting Information). Stable cycling performance was also achieved, in which capacities of  $117.9$  and  $94.4 \text{ mA h g}^{-1}$  maintained after 100 cycles with 84.1% and 85.6% capacity retention for P-TS and P-MS, respectively (Figure S17b, Supporting Information). Furthermore, O-ECIC systems can also be applied to multivalent ion batteries. In rechargeable Mg batteries (Figure S18, Supporting Information) and rechargeable Al batteries (Figure S19, Supporting Information), P-MS electrodes deliver capacities of  $97.5$  and  $88.6 \text{ mA h g}^{-1}$ , respectively, both of which are higher than those of PTCDA/carbon electrodes. Our proposed O-ECIC system can be used as a general strategy to enhance the capacity of organic-based electrodes not only in monovalent Li and Na batteries but also in divalent Mg and trivalent Al batteries.

In addition to PTCDA, HATN, another representative organic electrode material,<sup>[4d]</sup> can also be combined with ECIC to demonstrate the advantages of the O-ECIC system (Figure S20, Supporting Information). HATN- $\text{Mo}_6\text{S}_8$  (H-MS) electrode delivered a high capacity of  $121.5 \text{ mA h g}^{-1}$ , much higher than HATN/carbon electrodes ( $<90 \text{ mA h g}^{-1}$ ) (Figure S20a, Supporting Information). A high capacity of  $109.8 \text{ mA h g}^{-1}$  was maintained after 1000 cycles with a capacity retention of 88.4%, signifying

excellent cycling stability (Figure S20b, Supporting Information). The extension to HATN expands the universality of the O-ECIC system to more organic electrode materials.

In summary, we propose an O-ECIC strategy to achieve high-energy organic-based battery systems, in which ECIC transports electrons for the redox reaction of the entire electrodes, stores ions to act as secondary active materials, and has a strong affinity with OEMs to inhibit their dissolution. O-ECIC electrodes simultaneously achieve a high ratio of active materials (OEMs + ECIC), low porosity, lean electrolyte, and thus high energy density. Randomly combining two representative ECICs ( $\text{Mo}_6\text{S}_8$  and  $\text{TiS}_2$ ) with OEMs (PTCDA and HATN) improved the electrochemical performance in monovalent Li and Na batteries, divalent Mg batteries, and trivalent Al batteries. Both high specific energy ( $153 \text{ Wh kg}^{-1}$ ) and energy density ( $200 \text{ Wh L}^{-1}$ ) are delivered in a 30 mA h-level Li/P-TS pouch cell, which, to the best of our knowledge, is highly competitive with reported organic electrodes. Our proposed O-ECIC system provides a new paradigm to enhance the energy density of OEMs. This work will enable a big leap forward for the practical implementation of organic-based battery systems.

## Experimental Section

Material synthesis, material characterizations, electrochemical measurements, and calculation details are provided in the Supporting Information.

## Supporting Information

Supporting Information is available from the Wiley Online Library or from the author.

## Acknowledgements

M.M. and S.W. contributed equally to this work.

## Conflict of Interest

The authors declare no conflict of interest.

## Keywords

electronic conductive inorganic cathodes, high energy, lean electrolytes, low porosity, organic electrode materials

Received: August 25, 2020

Revised: December 10, 2020

Published online:

[1] a) A. Jain, S. P. Ong, G. Hautier, W. Chen, W. D. Richards, S. Dacek, S. Cholia, D. Gunter, D. Skinner, G. Ceder, K. A. Persson, *APL Mater.* **2013**, *1*, 011002; b) M. S. Whittingham, *Chem. Rev.* **2014**, *114*, 11414; c) J. B. Goodenough, Y. Kim, *Chem. Mater.* **2010**, *22*, 587.

- [2] a) S. Muench, A. Wild, C. Fribe, B. Häupler, T. Janoschka, U. S. Schubert, *Chem. Rev.* **2016**, *116*, 9438; b) Y. Liang, Y. Yao, *Joule* **2018**, *2*, 1690.
- [3] a) T. B. Schon, B. T. McAllister, P.-F. Li, D. S. Seferos, *Chem. Soc. Rev.* **2016**, *45*, 6345; b) Y. Lu, Q. Zhang, L. Li, Z. Niu, J. Chen, *Chem.* **2018**, *4*, 2786; c) H. B. Wu, X. W. Lou, *Sci. Adv.* **2017**, *3*, 9252; d) C. Kim, H. Ejima, N. Yoshie, *J. Mater. Chem. A* **2018**, *6*, 19643.
- [4] a) C. Peng, G.-H. Ning, J. Su, G. Zhong, W. Tang, B. Tian, C. Su, D. Yu, L. Zu, J. Yang, M.-F. Ng, Y.-S. Hu, Y. Yang, M. Armand, K. Loh, *Nat. Energy* **2017**, *2*, 17074; b) Z. Luo, L. Liu, Q. Zhao, F. Li, J. Chen, *Angew. Chem., Int. Ed.* **2017**, *56*, 12561; c) M. Lee, J. Hong, J. Lopez, Y. Sun, D. Feng, K. Lim, W. C. Chueh, M. F. Toney, Y. Cui, Z. Bao, *Nat. Energy* **2017**, *2*, 861; d) M. Mao, C. Luo, T. P. Pollard, S. Hou, T. Gao, X. Fan, C. Cui, J. Yue, Y. Tong, G. Yang, T. Deng, M. Zhang, J. Ma, L. Suo, O. Borodin, C. Wang, *Angew. Chem., Int. Ed.* **2019**, *58*, 17820; e) Z. Song, H. Zhou, *Energy Environ. Sci.* **2013**, *6*, 2280; f) Y. Liang, Z. Tao, J. Chen, *Adv. Energy Mater.* **2012**, *2*, 742.
- [5] a) J. Wang, C. S. Chen, Y. Zhang, *ACS Sustainable Chem. Eng.* **2018**, *6*, 1772; b) J. Xie, Q. Zhang, *J. Mater. Chem. A* **2016**, *4*, 7091.
- [6] a) W. Luo, M. Allen, V. Raju, X. Ji, *Adv. Energy Mater.* **2014**, *4*, 1400554; b) X. Wang, C. Bommier, Z. Jian, Z. Li, R. S. Chandrasebose, I. A. Rodríguez-Pérez, P. A. Greaney, X. Ji, *Angew. Chem., Int. Ed.* **2017**, *56*, 2909.
- [7] M.-J. Lee, S. Lee, P. Oh, Y. Kim, J. Cho, *Nano Lett.* **2014**, *14*, 993.
- [8] J. Barker, M. Y. Saidi, R. K. B. Gover, P. Burns, A. Bryan, *J. Power Sources* **2007**, *174*, 927.
- [9] J.-N. Zhang, Q. Li, C. Ouyang, X. Yu, M. Ge, X. Huang, E. Hu, C. Ma, S. Li, R. Xiao, W. Yang, Y. Chu, Y. Liu, H. Yu, X.-Q. Yang, X. Huang, L. Chen, H. Li, *Nat. Energy* **2019**, *4*, 594.
- [10] A. Yamada, S. C. Chung, K. Hinokuma, *J. Electrochem. Soc.* **2001**, *148*, A224.
- [11] a) S. Xu, G. Wang, B. P. Biswal, M. Addicoat, S. Paasch, W. Sheng, X. Zhuang, E. Brunner, T. Heine, R. Berger, X. Feng, *Angew. Chem., Int. Ed.* **2019**, *58*, 849; b) P. Sharma, D. Damien, K. Nagarajan, M. M. Shajumon, M. Hariharan, *J. Phys. Chem. Lett.* **2013**, *4*, 3192; c) F. Jing, T. Huang, G. Tao, L. Ma, D. Lu, R. Liu, X. Xi, D. Wu, *Electrochim. Acta* **2018**, *276*, 207; d) L. Z. Zhan, Z. P. Song, J. Y. Zhang, J. Tang, H. Zhan, Y. H. Zhou, C. M. Zhan, *J. Appl. Electrochem.* **2008**, *38*, 1691; e) Z. Luo, L. Liu, J. Ning, K. Lei, Y. Lu, F. Li, J. Chen, *Angew. Chem., Int. Ed.* **2018**, *57*, 9443; f) Z. Song, H. Zhan, Y. Zhou, *Chem. Commun.* **2009**, *448*; g) X. Fan, F. Wang, X. Ji, R. Wang, T. Gao, S. Hou, J. Chen, T. Deng, X. Li, L. Chen, C. Luo, L. Wang, C. Wang, *Angew. Chem., Int. Ed.* **2018**, *57*, 7146; h) C. Luo, O. Borodin, X. Ji, S. Hou, K. J. Gaskell, X. Fan, J. Chen, T. Deng, R. Wang, J. Jiang, C. Wang, *Proc. Natl. Acad. Sci. USA* **2018**, *115*, 2004; i) B. Tian, Z. Ding, G.-H. Ning, W. Tang, C. Peng, B. Liu, J. Su, C. Su, K. P. Loh, *Chem. Commun.* **2017**, *53*, 2914; j) S. Wang, L. Wang, K. Zhang, Z. Zhu, Z. Tao, J. Chen, *Nano Lett.* **2013**, *13*, 4404.
- [12] A.-M. Cao, J.-S. Hu, H.-P. Liang, L.-J. Wan, *Angew. Chem., Int. Ed.* **2005**, *44*, 4391.
- [13] L. Zhou, L. Yang, P. Yuan, J. Zou, Y. Wu, C. Yu, *J. Phys. Chem. C* **2010**, *114*, 21868.
- [14] B. Zachau-Christiansen, K. West, T. Jacobsen, S. Atlung, *Solid State Ion.* **1988**, *28–30*, 1176.
- [15] N. Imanishi, *J. Electrochem. Soc.* **1992**, *139*, 2082.
- [16] a) Y. Liao, K.-S. Park, P. Singh, W. Li, J. B. Goodenough, *J. Power Sources* **2014**, *245*, 27; b) J. Zhu, H. N. Alshareef, U. Schwingenschlögl, *Appl. Phys. Lett.* **2017**, *111*, 043903.
- [17] X. Fang, C. Hua, C. Wu, X. Wang, L. Shen, Q. Kong, J. Wang, Y. Hu, Z. Wang, L. Chen, *Chem. - Eur. J.* **2013**, *19*, 5694.
- [18] a) M. Mao, Z. Lin, Y. Tong, J. Yue, C. Zhao, J. Lu, Q. Zhang, L. Gu, L. Suo, Y.-S. Hu, H. Li, X. Huang, L. Chen, *ACS Nano* **2020**, *14*, 1102; b) W. Xue, Z. Shi, L. Suo, C. Wang, Z. Wang, H. Wang, K. P. So, A. Maurano, D. Yu, Y. Chen, L. Qie, Z. Zhu,

G. Xu, J. Kong, J. Li, *Nat. Energy* **2019**, *4*, 374; c) W. Xue, D. Yu, L. Suo, C. Wang, Z. Wang, G. Xu, X. Xiao, M. Ge, M. Ko, Y. Chen, L. Qie, Z. Zhu, A. S. Helal, W.-K. Lee, J. Li, *Matter* **2019**, *1*, 1047.

[19] R. Winter, P. Heitjans, *J. Phys. Chem. B* **2001**, *105*, 6108.

[20] T. Yamamoto, *J. Electrochem. Soc.* **1986**, *133*, 1558.

[21] a) T. R. Juran, M. Smeu, *J. Power Sources* **2019**, *436*, 226813; b) P. Li, X. Zheng, H. Yu, G. Zhao, J. Shu, X. Xu, W. Sun, S. X. Dou, *Energy Storage Mater.* **2019**, *16*, 512.

[22] A. H. Thompson, J. C. Scanlon, C. R. Symon, *Solid State Ion* **1980**, *1*, 47.

[23] J. Molenda, *Solid State Ion* **2005**, *176*, 1687.

[24] F. Badway, A. N. Mansour, N. Pereira, J. F. Al-Sharab, F. Cosandey, I. Plitz, G. G. Amatucci, *Chem. Mater.* **2007**, *19*, 4129.

[25] Y. H. Chen, C. W. Wang, G. Liu, X. Y. Song, V. S. Battaglia, A. M. Sastry, *J. Electrochem. Soc.* **2007**, *154*, A978.

[26] P. Poizot, J. Gaubicher, S. Renault, L. Dubois, Y. Liang, Y. Yao, *Chem. Rev.* **2020**, *120*, 6490.